

Dose-dependent effects of enzyme replacement therapy on skeletal disease progression in mucopolysaccharidosis VII dogs

Rahul Gawri,^{1,2,8} Yian Khai Lau,^{1,2,8} Gloria Lin,³ Snehal S. Shetye,¹ Chenghao Zhang,^{1,2} Zhirui Jiang,^{1,2} Khaled Abdoun,^{1,2} Carla R. Scanzello,^{4,5} Stephanie Y. Jo,⁶ Wilfried Mai,⁷ George R. Dodge,¹ Margret L. Casal,³ and Lachlan J. Smith^{1,2}

¹Department of Orthopaedic Surgery, Perelman School of Medicine, University of Pennsylvania, Philadelphia, PA, USA; ²Department of Neurosurgery, Perelman School of Medicine, University of Pennsylvania, Philadelphia, PA, USA; ³Department of Clinical Sciences and Advanced Medicine, Section of Medical Genetics, School of Veterinary Medicine, University of Pennsylvania, Philadelphia, PA, USA; ⁴Department of Medicine, Perelman School of Medicine, University of Pennsylvania, Philadelphia, PA, USA; ⁵Department of Medicine, Corporal Michael J. Crescenz VA Medical Center, Philadelphia, PA, USA; ⁶Department of Radiology, Perelman School of Medicine, University of Pennsylvania, Philadelphia, PA, USA; ⁷Department of Clinical Sciences and Advanced Medicine, Section of Radiology, School of Veterinary Medicine, University of Pennsylvania, Philadelphia, PA, USA

Mucopolysaccharidosis (MPS) VII is an inherited lysosomal storage disorder characterized by deficient activity of the enzyme β -glucuronidase. Skeletal abnormalities are common in patients and result in diminished quality of life. Enzyme replacement therapy (ERT) for MPS VII using recombinant human β -glucuronidase (vestronidase alfa) was recently approved for use in patients; however, to date there have been no studies evaluating therapeutic efficacy in a large animal model of MPS VII. The objective of this study was to establish the effects of intravenous ERT, administered at either the standard clinical dose (4 mg/kg) or a high dose (20 mg/kg), on skeletal disease progression in MPS VII using the naturally occurring canine model. Untreated MPS VII animals exhibited progressive synovial joint and vertebral bone disease and were no longer ambulatory by age 6 months. Standard-dose ERT-treated animals exhibited modest attenuation of joint disease, but by age 6 months were no longer ambulatory. High-dose ERT-treated animals exhibited marked attenuation of joint disease, and all were still ambulatory by age 6 months. Vertebral bone disease was recalcitrant to ERT irrespective of dose. Overall, our findings indicate that ERT administered at higher doses results in significantly improved skeletal disease outcomes in MPS VII dogs.

INTRODUCTION

The mucopolysaccharidoses (MPS) are a family of lysosomal storage disorders characterized by deficient activity of enzymes that degrade glycosaminoglycans (GAGs) due to gene mutations.¹ The combined prevalence of MPS across all 11 subtypes is estimated to be approximately 1 per 100,000 live births in the US.² MPS VII, also called Sly syndrome, is characterized by deficient activity of the enzyme β -glucuronidase (GUSB), leading to aberrant accumulation of incompletely degraded chondroitin, dermatan, and heparan sulfate GAGs.³

Patients with MPS VII exhibit multi-organ disease manifestations, including in the cardio-pulmonary, central nervous, and musculoskeletal systems.³⁻⁵ Musculoskeletal manifestations (dysostosis multiplex) are prevalent and occur in both the spine and synovial joints, resulting in chronic pain and impaired mobility that negatively impact patient quality of life.⁴ Spine disease is characterized by progressive kypho-scoliotic deformity, which is due in part to failures of endochondral bone formation in the vertebrae during postnatal growth.⁶⁻⁸ Synovial joint disease commonly manifests as stiffness and limited range of motion.⁴ While the underlying mechanisms of spine and joint disease in MPS VII remain incompletely understood, animal studies suggest that from an early age abnormal GAG accumulation in chondrocytes, osteoblasts and osteocytes,⁹ and in the extracellular matrix,¹⁰ drives impaired bone formation in the vertebrae and long bones,^{10,11} and inflammatory degenerative changes in the joints.^{12,13}

Enzyme replacement therapy (ERT) is the standard of care treatment for several MPS subtypes, including I, II, IVA, VI, and VII.¹⁴ Treatment typically involves patients receiving regular (e.g., biweekly) intravenous infusions of exogenous enzyme. The first report of an MPS VII patient treated with ERT using recombinant human GUSB was in 2015,¹⁵ and ERT (vestronidase alfa) was approved for clinical use in the US by the Food and Drug Administration in

Received 22 August 2022; accepted 21 November 2022;
<https://doi.org/10.1016/j.omtm.2022.11.006>.

*These authors contributed equally

Correspondence: Margret L. Casal, Department of Clinical Sciences and Advanced Medicine, Section of Medical Genetics, School of Veterinary Medicine, University of Pennsylvania, Philadelphia, PA, USA.
E-mail: casalml@vet.upenn.edu

Correspondence: Lachlan J. Smith, Department of Orthopaedic Surgery, Perelman School of Medicine, University of Pennsylvania, Philadelphia, PA, USA.
E-mail: lachlans@penncmedicine.upenn.edu



2017.¹⁶ There is limited information from early clinical studies and case reports on how effective ERT is for treating the skeletal manifestations of MPS; however, it has been reported that some MPS VII patients receiving ERT exhibit improvements in growth, joint range of motion and mobility, suggesting a positive effect on skeletal disease.^{16,17} Studies in MPS VII mice suggest that ERT ameliorates, at least partially, skeletal pathology and improves bone growth, but the administered enzyme does not reach all involved cell types.¹⁸

Naturally occurring large animal models of MPS represent powerful, clinically relevant platforms to study skeletal disease pathogenesis and response to therapy.¹⁹ Compared with mouse models, large animal models have more genetic diversity, and more closely recapitulate the pathological characteristics and rate of progression of skeletal disease that occurs in human patients. MPS VII dogs, specifically, exhibit progressive vertebral body and synovial joint abnormalities, and declining mobility over time, making them excellent analogs for the human disease.^{8,11,20,21} Furthermore, due to their longer lifespan, large animal models facilitate long-term treatment studies with efficacy assessed through gold standard, clinically relevant outcome measures. Previously, effects of ERT on skeletal disease progression have been studied in MPS I and VI using dogs and cats, respectively^{22,23}; however, to date, there have been no studies evaluating ERT efficacy in any large animal models of MPS VII.

The objective of this study was to evaluate the efficacy of intravenous ERT using vestronidase alfa for treating skeletal disease in MPS VII using the naturally occurring canine model. MPS VII dogs were treated from birth to age 6 months using either the standard clinical dose of 4 mg/kg or a high dose of 20 mg/kg. In addition to assessing systemic effects, outcome measures focused on evaluating improvements in synovial joints and vertebral bones, as these are defining characteristics of skeletal disease in both canine and human MPS VII, and are associated with a profound clinical decline in mobility and quality of life.

RESULTS

Clinical findings

MPS VII dogs were treated with intravenous vestronidase alfa beginning at age 2 days. Two doses were evaluated: the standard clinical dose of 4 mg/kg (“MPS VII ERT SD”) and a high dose of 20 mg/kg (“MPS VII ERT HD”). Study groups also included untreated MPS VII animals (“MPS VII Untreated”) and healthy controls (“Controls”). All animals completed the study successfully without serious adverse events and no unexpected deaths were recorded. Based on pilot studies, a prophylactic drug regimen consisting of an antihistamine and two antiemetics was developed to prevent mild to moderate adverse reactions, which included rash, vomiting, and diarrhea during infusions. Furthermore, to prevent persistent adverse reactions in animals receiving the high ERT dose, a steroid was administered before each infusion for this group only. To confirm that administration of this steroid did not confound interpretation of ERT findings, an additional control group of MPS VII animals (“MPS VII Steroid Control”) was included, which received all prophylactic drugs but not ERT.

Complete physical examinations were performed monthly and focused on assessing overall animal health as well as muscle tone, joint swelling, and ability to ambulate. Comprehensive findings are provided as supplemental data, and skeletal findings are summarized in [Table S1](#). Rate of weight gain was lower for all MPS VII animals compared with controls, regardless of treatment ([Figure S1](#)). At age 4, 5, and 6 months, weights were significantly lower than controls for untreated MPS VII animals. For healthy controls, physical examinations revealed normal growing animals with no abnormalities. At age 6 months, all were lively and had normal gaits. In contrast, all untreated MPS VII animals exhibited physical manifestations by age 2–4 weeks, including facial dysmorphism. By age 2 months, effusions in carpal and tarsal joints were evident, with all animals but one still ambulatory. By age 3 months, palpable joint effusions were also present in elbows and stifles, and all animals had trouble rising with poor muscle tone over the lumbar spine and hindlimbs. Gait abnormalities became evident in animals that were still ambulatory. By the end of 4 months no untreated MPS VII animals were able to rise without assistance, and by age 5 months none were ambulatory. For some animals, elbows and hips felt subluxated on palpation, and by age 6 months all had severe joint effusions in all limbs.

MPS VII ERT SD animals generally exhibited similar disease manifestations to untreated animals; however, disease overall progressed more slowly, with facial dysmorphism first evident around age 1 month. By 3 months, joint effusions were present in the carpi of most and in the elbows of one animal, muscle wasting was noted in one animal, while all remained ambulatory. At age 4 months, all ERT SD animals exhibited stunted growth and muscle wasting across their pelvic spine and hindlimbs, while joint effusions ranged from mild to moderate in all but one animal. Two animals were still ambulatory, while three had difficulty rising and limited mobility. By age 5 months, one animal still had very little joint effusion and was still ambulatory, one was able to stand and walk with assistance, while the remainder could not. By age 6 months, all ERT SD animals were unable to stand or ambulate independently and were subjectively similar in appearance to the MPS VII untreated animals, with the exception of one animal that had very little joint effusion.

In contrast, MPS VII ERT HD animals exhibited generally mild disease manifestations through the 6 months study course. At age 1 month, all of these animals exhibited normal appearance. By age 2 months, two animals appeared mildly affected, while the third appeared normal. All were ambulatory with no difficulties, and one had very mild effusion in the right carpal joint. By age 3 months, mild effusions were present in the carpal and/or tarsal joints of two animals. At age 6 months, all animals remained ambulatory and were very bright, lively, and alert. Two animals exhibited slightly stunted growth and showed mild signs of lameness at the study endpoint, while the third animal had completely normal gait.

Finally, progression of disease in MPS VII steroid control animals was subjectively similar to untreated MPS VII animals. At age 1 month, all animals exhibited facial dysmorphism. By age 2 months, two animals

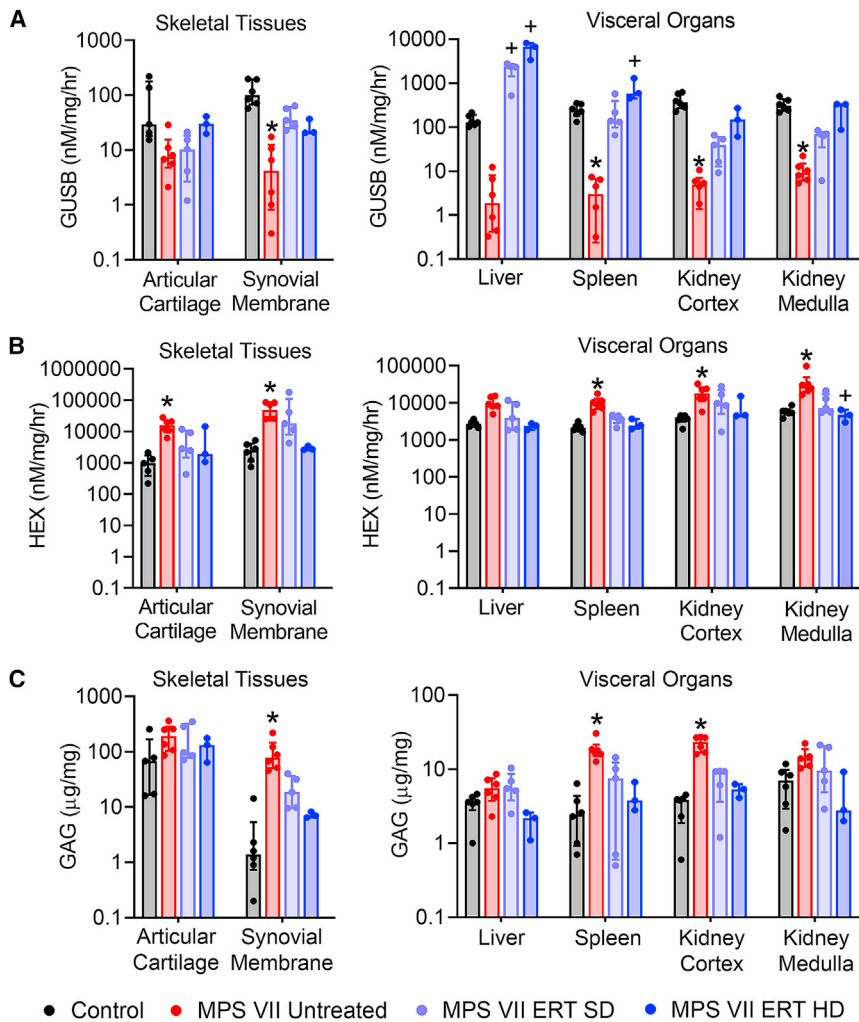


Figure 1. Tissue enzyme distribution and glycosaminoglycan content for skeletal tissues and visceral organs

(A) β -Glucuronidase (GUSB) activity, (B) β -hexosaminidase (HEX) activity, and (C) glycosaminoglycan (GAG) content. Results are normalized to total protein content. * $p < 0.05$ versus Control; + $p < 0.05$ versus MPS VII Untreated; $n = 3-6$ per group; Kruskal-Wallis tests with post-hoc Dunn's tests. Data are presented as median and interquartile range.

tissues examined, ranging from 0.79% of control in the brain stem to 25.14% of control in articular cartilage. Differences were statistically significant for all tissues except articular cartilage and liver. For most tissues, ERT-treated MPS VII dogs exhibited higher GUSB activity compared with MPS VII untreated animals, and which was not significantly different from controls. For most tissues results were dose dependent, with the highest enzyme activity found for MPS VII ERT HD animals. As an indirect measure of GUSB penetration and cellular uptake, β -hexosaminidase (HEX) enzyme activity was also measured in representative tissues from major organ systems (Figures 1B and S3B). HEX is expected to be elevated in MPS VII as the enzyme is overexpressed as a compensatory mechanism to GUSB deficiency. Tissue-relative HEX activity was generally found to be the inverse of tissue GUSB activity, and was significantly elevated in untreated MPS VII animals compared with controls for all tissues except brain stem and

had flared ribs, all had effusions in their tarsal and carpal joints, one animal showed difficulty ambulating, while another was no longer able to rise and ambulate. The disease continued to progress until the study endpoint. Subluxation of the right elbow was noted in one animal by age 3 months and in another by 4 months. By 5 months, effusion in limb joints was pronounced, and none of these animals were able to stand or ambulate. Loss of muscle mass was evident over the caudal spine and the hindlimbs.

Blood was collected before euthanasia at age 6 months for complete blood counts. There were no significant differences in the total number of white blood cells, or relative numbers of neutrophils, lymphocytes, monocytes, or platelets between study groups (Figures S2A–S2E).

Tissue enzyme distribution and GAG content

To establish the efficacy of enzyme distribution in treated animals, GUSB activity was measured in representative tissues from major organ systems (Figures 1A and S3A). As expected, GUSB activity for untreated MPS VII animals was diminished relative to controls for all

liver, ranging from 321% of control in the liver, to 1953% of control in synovial membrane. For MPS VII ERT (SD and HD) animals, HEX activity was lower than MPS VII untreated for all tissues (not significantly different from control), with the greatest reduction observed for ERT HD animals, where activity was similar to controls.

As a direct measure of ERT efficacy, GAG content was also determined in representative tissues from major organ systems and serum (Figures 1C and S3C). GAG content was elevated for MPS VII untreated animals compared with controls for all tissues ($p < 0.05$ for synovial membrane, ascending and descending aorta, spleen, and kidney cortex), ranging from 138% of control in the thoracic spinal cord to 6,147% of control in the ascending aorta. For MPS VII ERT animals, GAG levels were reduced, and not significantly different from control for any tissues. A dose-dependent response to ERT was observed for most tissues, with a greater reduction in GAG content for ERT HD animals compared with ERT SD animals. In serum, GAG content was significantly lower in ERT HD animals compared with MPS VII untreated animals (Figure S3C).

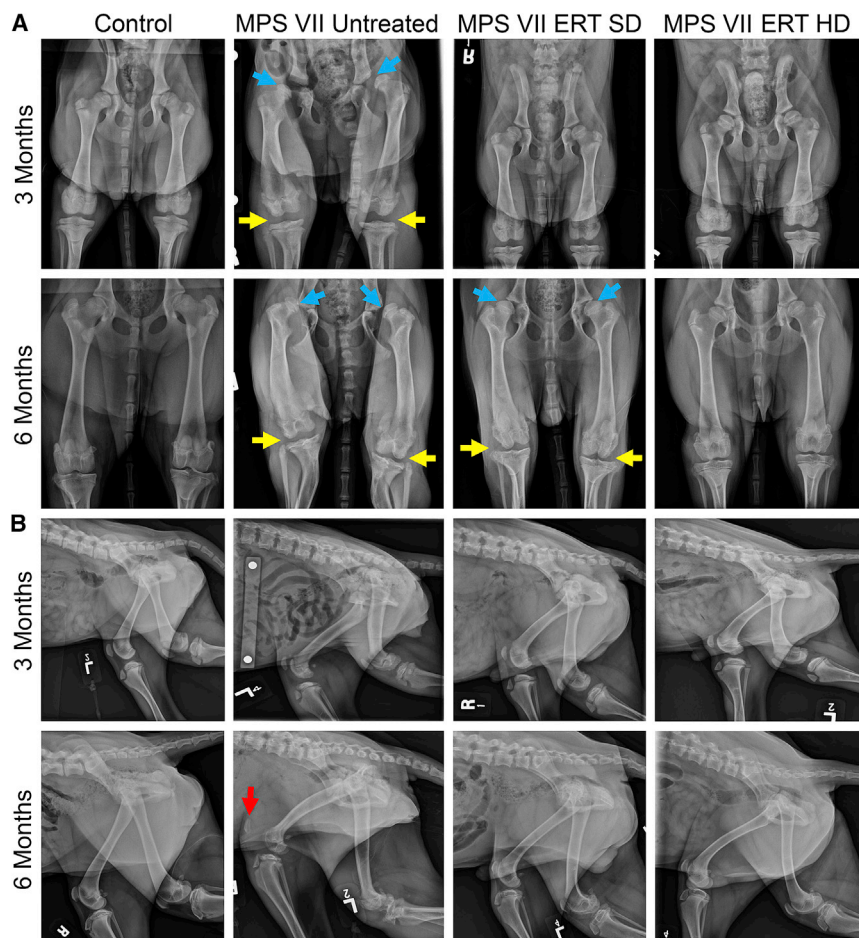


Figure 2. Plain radiographs of the lower appendicular skeleton

(A) Ventrodorsal and (B) lateral views at age 3 and 6 months. The blue arrows indicate coxofemoral subluxation, the yellow arrows indicate genu valgum and the red arrow indicates patellar dislocation. Joint abnormalities exhibited dose-dependent improvements with ERT.

Effects of treatment on synovial joint disease

Stifle joint structural abnormalities were assessed using *in vivo* plain radiographs obtained at age 3 and 6 months, and postmortem magnetic resonance imaging (MRI). Findings from plain radiographs are summarized in Table S2, with representative images shown in Figure 2. Shallow or irregular acetabula, and femoral epiphyseal irregularities were noted for most MPS VII-affected animals regardless of treatment status. In contrast, genu valgum, tibial bowing, limb muscle atrophy, and coxofemoral subluxation, while present in most untreated MPS VII and steroid control animals, were absent in the majority of ERT-treated animals (SD and HD). The exception was coxofemoral subluxation, which manifested in all ERT SD animals (but not ERT HD animals) by age 6 months. MPS VII steroid control animals exhibited similar radiological features to untreated animals at age 6 months (Figure S4; Table S2).

Representative sagittal and dorsal (coronal) MRI images from each study group are shown in Figures 3A and 3B. Pathological features observed in untreated MPS VII animals included large synovial fluid effusions that in most cases extended to the caudal (posterior) of the joint as Baker's cysts. Associated with these effusions, the patellar was

frequently displaced from the femoral patellar groove. Meniscal extrusions and mid-substance degeneration, and infrapatellar fat pad synovitis, were also frequently noted in MPS VII untreated animals, while bone marrow edema, subchondral cysts, and articular cartilage irregularities were also occasionally observed. Semi-quantitative grading was used to evaluate joint pathology in response to treatment (Figures 3C–3L). For MPS VII untreated animals, effusion synovitis, Baker's cysts, fat pad synovitis, meniscal extrusion, patellar dislocation, subchondral cysts, and overall MRI grade were all significantly worse than control animals. For MPS VII ERT SD animals, there were non-significant improvements in most parameters assessed, while the greatest improvements occurred for MPS VII ERT HD animals, for which effusion synovitis, Baker's cysts, meniscal extrusion, fat pad synovitis, patellar displacement, and overall MRI grade were all significantly improved compared with MPS VII untreated animals. With respect to MPS VII

steroid control animals, stifle joints subjectively exhibited effusion synovitis and Baker's cysts, although patellar displacement and meniscal extrusion were milder or absent (Figure 3). Semi-quantitative grading demonstrated that bone marrow edema was significantly worse in steroid control animals compared with controls (Figure 3I). Collectively, these imaging findings are consistent with dose-dependent positive effects of ERT on preservation of joint structure, with some bone abnormalities persisting in treated animals.

The effects of treatment on articular cartilage from the mid-sagittal plane of the medial femoral condyle of the stifle were evaluated histologically. Qualitatively, cartilage from MPS VII untreated animals exhibited marked but spatially heterogeneous proteoglycan loss and chondrocyte pathology (increased density and clustering, Figures 4A and 4B). The morphology of the condyles from untreated MPS VII animals was markedly abnormal. Cartilage and condyle morphology from animals treated at both ERT doses appeared subjectively improved, although there was significant variability observed within groups. Semi-quantitative grading (Figures 4C–4F) revealed significantly worse chondrocyte pathology and overall grades for MPS VII untreated and ERT SD animals compared with controls.

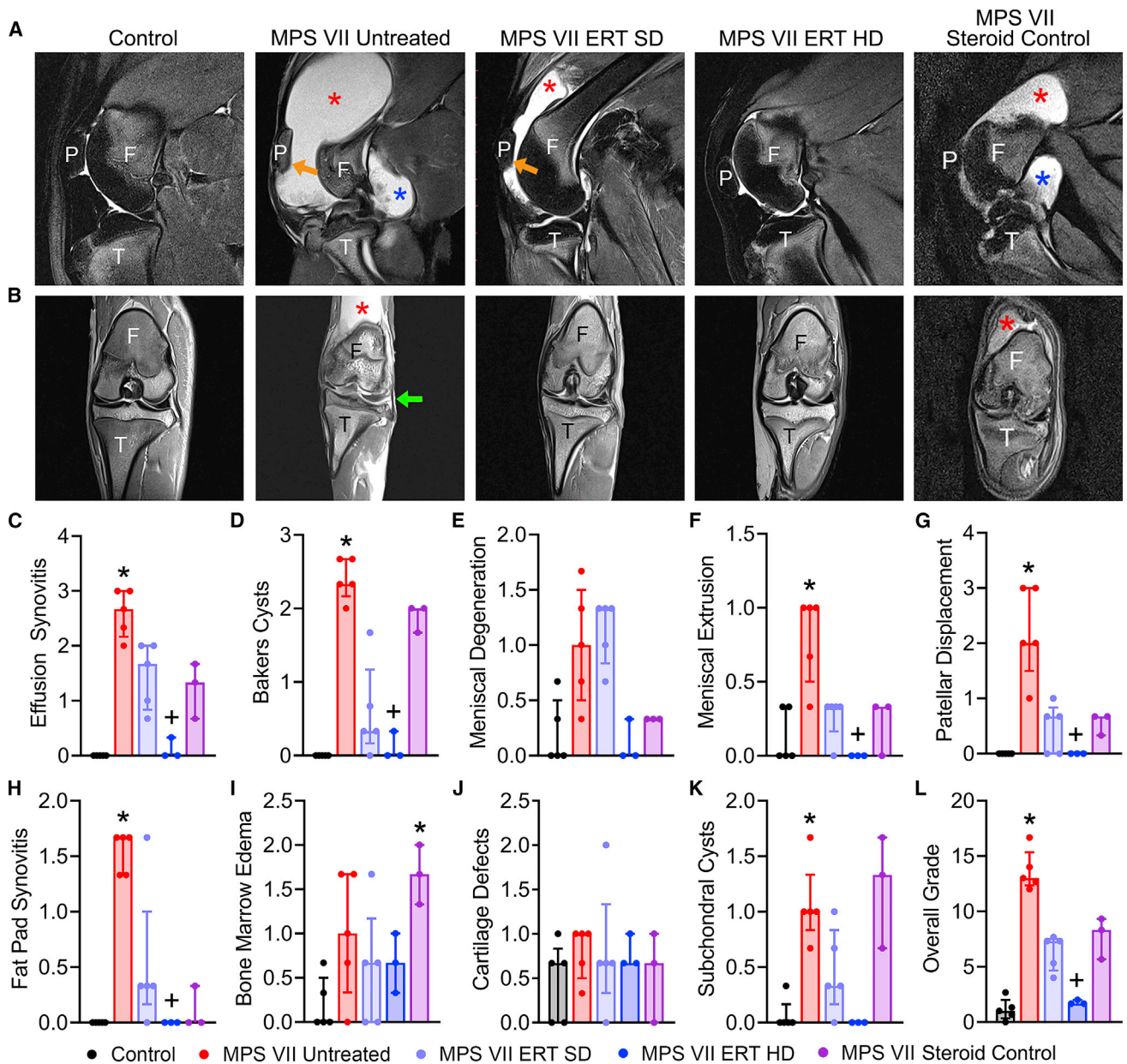


Figure 3. Magnetic resonance imaging of stifle joints

(A) Representative sagittal T2-weighted, fat saturated and (B) dorsal (coronal) proton density-weighted images illustrating pathological features of synovial joint disease in MPS VII dogs, including effusion synovitis cranial to the joint (red asterisks), Baker's cysts caudal to the joint (blue asterisks), patellar displacement (orange arrows), and meniscal extrusion (green arrow). Joint abnormalities exhibited dose-dependent improvements with ERT. F, femur (distal); T, tibia (proximal); P, patella. (C-L) Semi-quantitative grading of pathological features assessed from MRI images. Overall grade is the sum of individual scores. *p < 0.05 versus Control; +p < 0.05 versus MPS VII Untreated; n = 3-5 per group; Kruskal-Wallis tests with post-hoc Dunn's tests. Data are presented as median and interquartile range.

Relative expression of inflammatory mediators in synovial fluid (Figure 5) and serum (Figure S5) were measured using multiplex immunoassays. With respect to synovial fluid (Figure 5), of the 30 molecules that were detectable, 10 exhibited significantly different expression levels between study groups. Specifically, MMP-3, osteocalcin, osteopontin, gp130, IL-12, IL-29, and IL-11 were all significant elevated for

MPS VII untreated animals compared with controls. In MPS VII HD animals, expression levels of osteocalcin, osteopontin, and IL-12 were significantly lower than for untreated MPS VII animals and not significantly different from controls. In addition, expression levels of TNFSF13B, IL-26, and IL-35 were significantly lower than untreated MPS VII. Similar reductions in expression of inflammatory

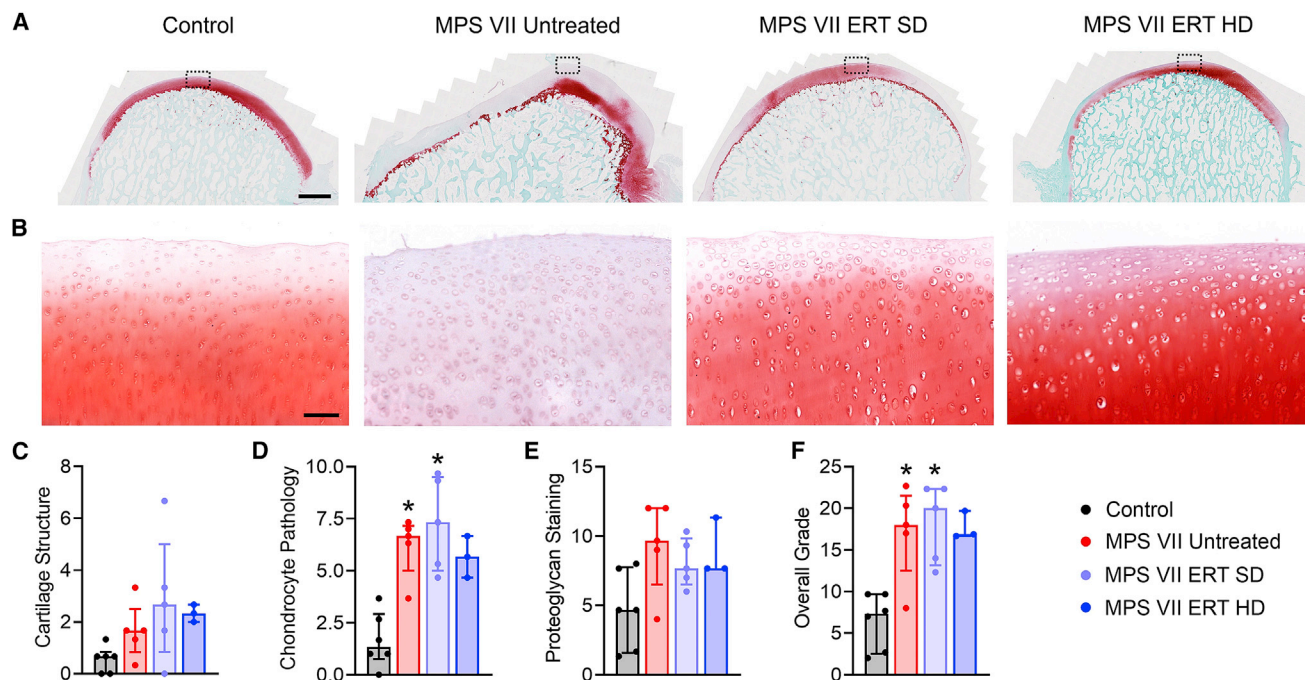


Figure 4. Histological evaluation of stifle joint articular cartilage

(A) Representative mid-sagittal sections of the medial femoral condyle. Scale bars, 2 mm (safranin-O and fast green stain). (B) Higher-magnification views of the regions indicated by the box in (A). Scale bar, 100 μ m. (C–F) Semi-quantitative grading of cartilage pathology. Overall grade is the sum of individual grades. * $p < 0.05$ versus Control; $n = 3$ –5 per group; Kruskal-Wallis tests with post-hoc Dunn's tests. Data are presented as median and interquartile range.

mediators were not evident for MPS VII ERT SD animals. With respect to serum (Figure S5), of the 26 molecules that were detectable, only 3 exhibited significant differences in expression between study groups. These included gp130 and MMP-2, both of which were significantly lower in MPS VII ERT HD compared with MPS VII untreated animals, and MMP-1, which was significantly elevated in MPS VII ERT HD compared with control animals.

Finally, to determine the effects of treatment on joint function, the biomechanical properties of the cranial cruciate ligament (CCL) (equivalent to the anterior cruciate ligament in humans) were tested to failure in uniaxial tension using a servo-hydraulic mechanical testing system (Figure 6A). The CCL performs a critical role in maintaining the rotational stability of the knee. CCLs from untreated MPS VII dogs exhibited significantly lower stiffness, modulus, failure stress, failure load, and toughness compared with controls (Figures 6B–6G). ERT treatment (SD and HD) resulted in non-statistically significant improvements in each of these parameters compared with untreated animals, and none of them were significantly different from controls.

Effects of treatment on vertebral bone disease

Effects of ERT on vertebral bone disease were evaluated using *in vivo* plain radiographs at age 3 and 6 months, and postmortem microcomputed tomography (microCT) and histology. Findings from lateral plain radiographs of lumbar spines are summarized in Table S2 and

representative images are shown in Figure 7A. Vertebral abnormalities, including diminished longitudinal growth and underdevelopment of cranial and caudal epiphyses (Figure 7A, arrows), were noted for most animals in all study groups except controls at both ages. Postmortem microCT of T13 vertebrae (Figures 7B–7H) demonstrated that bone volume fraction was significantly lower than controls at age 6 months for MPS VII ERT SD, and not significantly different than untreated MPS VII. Bone mineral density (BMD) was significantly lower than controls at age 6 months for MPS VII ERT SD and HD, and not significantly different than untreated MPS VII. Similarly, bone architectural parameters, including trabecular thickness, spacing, and number, were not improved with treatment at either dose. Connectivity density was significantly lower for ERT SD animals compared with untreated MPS VII, and not significantly different than controls. Systemic effects on bone formation were evaluated through serum analysis of bone-specific alkaline phosphatase (BAP) (Figure 7I). BAP activity was significantly lower for MPS VII untreated animals compared with controls. For treated animals (SD and HD), BAP was not significantly different from either untreated MPS VII or control animals.

Finally, mid-sagittal sections of T13 vertebrae were evaluated histologically (Figure 8). Findings included diminished trabecular bone in primary ossification centers, and the presence of cartilaginous lesions in the peripheral regions of secondary ossification centers in vertebrae from MPS VII animals compared with controls. These

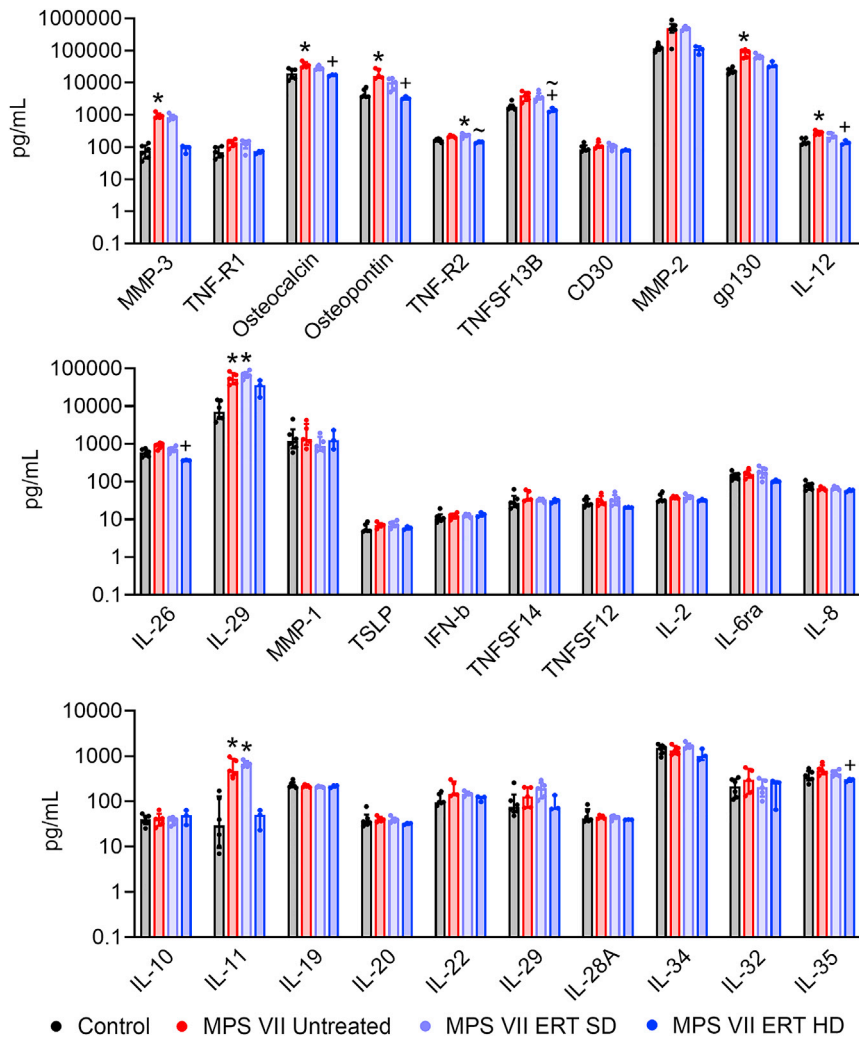


Figure 5. Expression levels of inflammatory mediators in synovial fluid

* $p < 0.05$ versus Control; + $p < 0.05$ versus MPS VII Untreated; ~ $p < 0.05$ versus MPS VII ERT SD; $n = 3-6$ per group; Kruskal-Wallis tests with post-hoc Dunn's tests. Data are presented as median and interquartile range.

velocity have been reported in some patients.^{16,17} Drawing conclusions on the skeletal response from these clinical studies is challenging given the broad spectrum of disease severity observed among study participants, and the limited number of patients available for study. An early preclinical study in newborn MPS VII mice found that intravenous GUSB administration resulted in improved long bone lengths and skull morphology, and reduced GAG storage in osteoblasts, but no such reduction in chondrocytes¹⁸; and, recently, it was shown that doses of vestronidase alfa up to 20 mg/kg administered to MPS VII mice resulted in higher relative enzyme activities in several tissues including kidney and lung, but not bone.²⁵

In this study, we found dose-dependent improvements in GUSB enzyme activity and corresponding reductions in GAG storage across multiple tissues, including those of abdominal visceral organs, and cardiovascular and central nervous systems. With respect to the skeleton, the results provide strong evidence of a dose-dependent positive effect of ERT on synovial joint disease. In untreated MPS VII animals, a rapid decline in mobility and inability to ambulate at all by the study endpoint was associated with pathological changes in all joint tissues examined, including large synovial effusions cranial and caudal to the joint, articular cartilage and meniscus degeneration, and diminished mechanical properties of CCLs. While modest joint improvements were observed for the standard ERT dose, at the high dose these improvements were profound and included complete normalization of synovial effusions. Remarkably, high-dose ERT resulted in near normal mobility at age 6 months. While we did not find a significant reduction in GAG content in articular cartilage with treatment at either dose, this was likely confounded by the fact that, in untreated MPS VII animals, this tissue exhibited localized proteoglycan depletion analogous to osteoarthritis, potentially as a consequence of local inflammation.

were not subjectively improved with ERT at either dose. Hematoxylin and eosin (H&E) staining revealed subjectively reduced cellularity in the vertebral growth plates for all MPS VII animals compared with controls, irrespective of treatment status. Quantitative analysis (Figures 8D–8G) revealed significantly lower cellularity in the proliferative zone of the growth plates of MPS VII untreated animals (Figure 8F), while for hypertrophic zone cellularity, and both proliferative and hypertrophic zone thicknesses, there were no significant differences between groups. Collectively, these results indicate that vertebral bone disease was unresponsive to ERT at either the standard clinical dose or the high dose.

DISCUSSION

Positive clinical findings reported to date in patients receiving vestronidase alfa include reductions in liver and spleen size, improved pulmonary function, decreased fatigue, and improvements in general overall wellbeing.^{15–17,24} While there is little data on the skeletal disease response, trends toward improved joint function and growth

late at all by the study endpoint was associated with pathological changes in all joint tissues examined, including large synovial effusions cranial and caudal to the joint, articular cartilage and meniscus degeneration, and diminished mechanical properties of CCLs. While modest joint improvements were observed for the standard ERT dose, at the high dose these improvements were profound and included complete normalization of synovial effusions. Remarkably, high-dose ERT resulted in near normal mobility at age 6 months. While we did not find a significant reduction in GAG content in articular cartilage with treatment at either dose, this was likely confounded by the fact that, in untreated MPS VII animals, this tissue exhibited localized proteoglycan depletion analogous to osteoarthritis, potentially as a consequence of local inflammation.

Elevated levels of inflammatory mediators in the synovial fluid of untreated MPS VII animals are consistent with the previously reported role of local inflammation in the progression of joint disease in several MPS subtypes.¹³ Expression levels of most of these molecules were

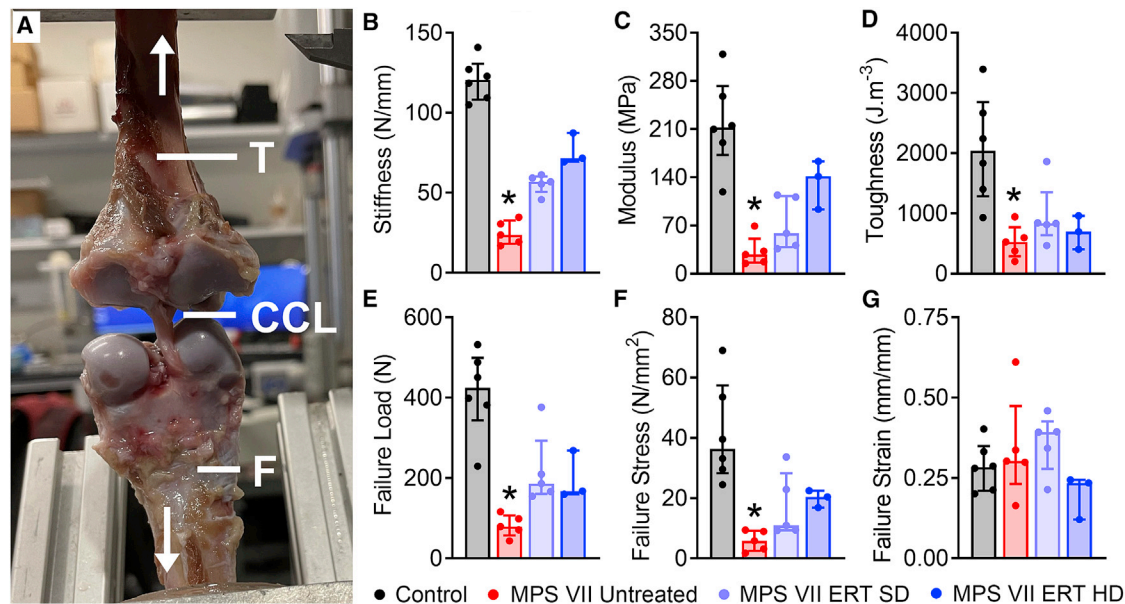


Figure 6. Biomechanical properties of CCLs

(A) Representative image of CCL undergoing uniaxial tensile testing. T, tibia (proximal); F, femur (distal); arrows, testing direction. (B) Stiffness, (C) modulus, (D) toughness, (E) failure load, (F) failure stress, (G) failure strain. * $p < 0.05$ versus Control; $n = 3-6$ per group; Kruskal-Wallis tests with post-hoc Dunn's tests. Data are presented as median and interquartile range.

reduced in animals that received high-dose ERT to levels approaching those of healthy controls. Notably, Gp130 is part of the IL-6 receptor complex, and elevated expression of IL-6 has been reported in patients with MPS I, where it was found to correlate with progressive changes in joint function.²⁶ IL-6 is upregulated in several other inflammatory joint diseases, including juvenile idiopathic arthritis (JIA), rheumatoid arthritis (RA), and osteoarthritis.²⁷⁻³⁰ IL-6 inhibition is already clinically approved for treatment of JIA and RA,^{27,29} and represents a possible supplementary therapeutic strategy for joint disease in MPS VII administered alongside ERT.

With respect to the vertebrae, untreated MPS VII animals exhibited similar pathological characteristics to those reported previously, including impaired secondary ossification, and diminished longitudinal vertebral growth, bone content, and mineral density in primary ossification centers, and altered cellularity in the growth plates.¹¹ In contrast to the positive findings seen in synovial joints, ERT resulted in no significant improvement in vertebral bone abnormalities, irrespective of dose. Contrasting findings for vertebral bone and synovial joints are similar to those reported in a previous study, in which MPS VII dogs were treated with hepatic retroviral gene therapy at birth, resulting in persistent, high levels of circulating enzyme.³¹ These animals exhibited a significant overall clinical improvement, including reduction in joint disease severity and long-term preservation of mobility,²¹ but had persistent vertebral bone abnormalities similar to untreated MPS VII animals.³² Potential reasons for the poor response of vertebrae to intravenous ERT may include the fact that bone and cartilage cells, including osteoblasts, osteocytes, and

epiphyseal and growth plate chondrocytes, exhibit significant storage from a very early age,⁹ and reside within dense, poorly vascularized tissues that may be inaccessible to circulating enzyme. Interestingly, these findings contrast with large animal ERT studies in other MPS subtypes. Specifically, intravenous alpha-L-iduronidase and arylsulfatase B administered to MPS I dogs and MPS VI cats, respectively, resulted in improvements in vertebral bone formation during postnatal growth.^{22,23} The reasons for these differences in efficacy across MPS subtypes are unknown, but possible explanations may include differences in enzyme size and structure that impact diffusion ability into bone and cartilage, differences in the type and number of GAG species that accumulate, and differential mechanisms of uptake among different cell types. Notably, in this study, a positive effect was seen on progression of facial dysmorphism, particularly in animals that received high-dose ERT, and this may suggest a greater therapeutic benefit on bones that form through intramembranous ossification compared with those that form through endochondral ossification.

Notably, organ systems other than the skeleton also exhibited dose-dependent improvements with ERT. Corneal clouding and heart murmurs evident in some or all of the untreated and standard-dose ERT animals were absent in high-dose ERT animals. Measured GUSB enzyme levels and corresponding reductions in GAG contents in cardiovascular and central nervous system tissues are also consistent with positive, systemic, dose-dependent effects of ERT.

Concerning safety, while no serious adverse events in response to vestronidase alfa administration were recorded during this study, mild to

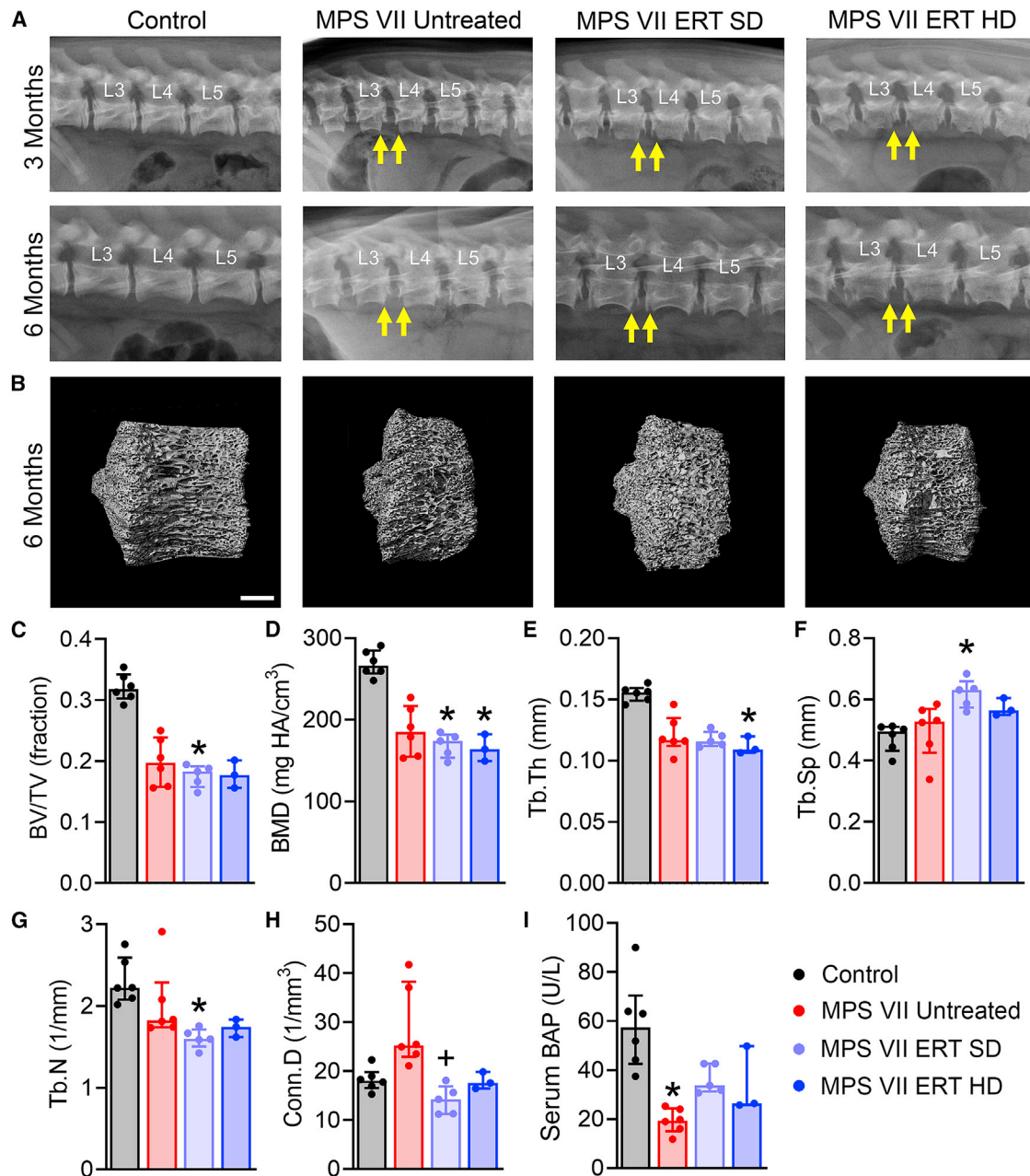


Figure 7. Plain radiographs and microCT imaging of vertebral bodies, and serum BAP activity

(A) Representative radiographs of lumbar spine vertebrae at age 3 and 6 months. Arrows indicate radiolucent lesions at the ventral margins, which were present in all MPS VII vertebrae regardless of treatment status. (B) Representative microCT images illustrating diminished longitudinal growth of MPS VII vertebral bodies at age 6 months regardless of treatment status. Scale bar, 3 mm. (C) Bone volume fraction (BV/TV), (D) bone mineral density (BMD), (E) trabecular thickness (Tb.Th), (F) trabecular spacing (Tb.Sp), (G) trabecular number (Tb.N), (H) connectivity density (Conn.Dens), (I) Serum BAP. * $p < 0.05$ versus Control; + $p < 0.05$ versus MPS VII Untreated; $n = 3-6$ per group; Kruskal-Wallis tests with post-hoc Dunn's tests. Data are presented as median and interquartile range.

moderate side effects, including rash, vomiting, and diarrhea, were common and necessitated the use of a prophylactic antihistamine and antiemetics. High-dose ERT animals required the additional administration of the steroid dexamethasone before each infusion to prevent these side effects. To assess potential anti-inflammatory ef-

fects of dexamethasone on joint findings, we evaluated joints in a separate cohort of animals that received dexamethasone without ERT. As noted in the [materials and methods](#), we were unable to obtain synovial fluid samples from steroid control animals, and we therefore cannot exclude the possibility that reductions in local

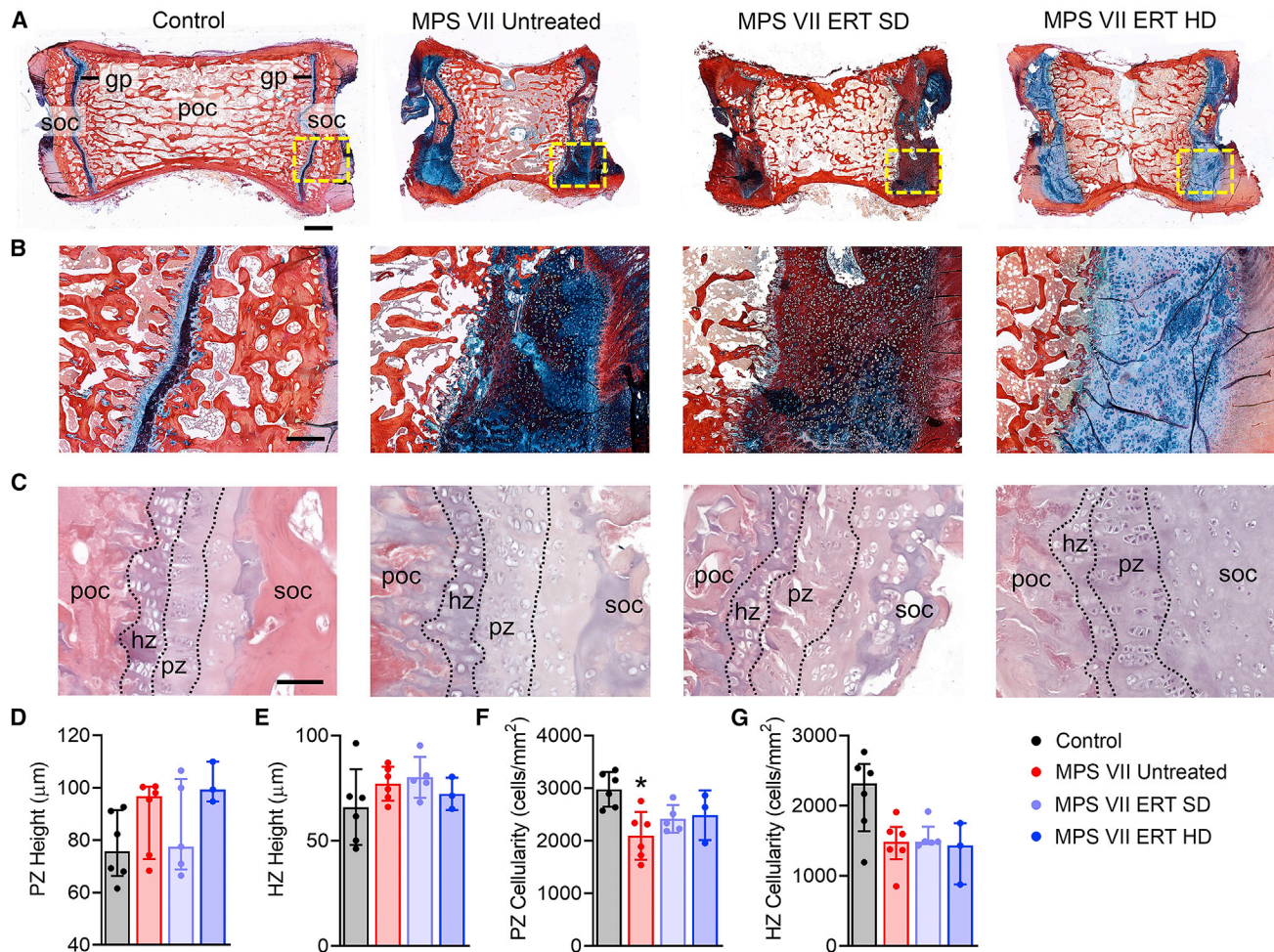


Figure 8. Histological evaluation of vertebral bodies

(A) Representative mid-sagittal sections of T13 vertebra illustrating diminished longitudinal growth and bone content in primary ossification centers (poc) of MPS VII vertebrae regardless of treatment status. Scale bar, 2 mm (Alcian blue and picosirius red stain). (B) Higher-magnification images of the regions indicated by boxes in (A), illustrating the presence of abnormal cartilage in the secondary ossification centers (soc) of MPS VII vertebrae, regardless of treatment status. Scale bar, 500 μm . (C) Representative mid-sagittal sections of vertebral growth plates illustrating diminished cellularity in MPS VII animals regardless of treatment status. Scale bar, 100 μm (hematoxylin and eosin stain). (D–G) Quantification of growth plate proliferative and hypertrophic zone (pz and hz, respectively) height and cellularity. * $p < 0.05$ versus Control; $n = 3\text{--}6$ per group; Kruskal-Wallis tests with post-hoc Dunn’s tests. Data are presented as median and interquartile range.

inflammatory mediator expression in high-dose ERT animals were due in part to the administration of dexamethasone. MRI suggested a modest reduction in joint pathology in steroid-only control animals; however, synovial effusions persisted, and mobility deficits progressed in these animals similarly to untreated MPS VII animals, supporting the conclusion that the positive effects observed in high-dose ERT animals were mainly due to ERT and not the steroid.

This study had several limitations. Firstly, the duration was limited to 6 months, and it will be important for future studies to establish whether the beneficial effects of ERT persist or are enhanced with longer-term treatment. Secondly, the sample sizes for some study groups were small, and the study was not sufficiently powered to

detect sex-dependent treatment effects. We hope to address this more comprehensively in the future. In addition, in this study ERT was started at birth before significant skeletal disease was present. As patients may not be diagnosed until they are several years old, it will be important to determine the efficacy of ERT commenced at older ages when skeletal disease is already progressed. Our findings add new weight to the case for neonatal screening for MPS VII to enable early diagnosis and therapeutic intervention for the best possible treatment outcomes.

In conclusion, in this study we undertook the first ever evaluation of vestronidase alfa in a large animal model of MPS VII. We demonstrated dose-dependent improvements in synovial joint disease and

mobility, while vertebral bone disease was recalcitrant to treatment irrespective of dose. These results suggest that there may be a clinical benefit to administering higher doses of vestronidase alfa in MPS VII patients with synovial joint disease that is not improved following treatment at the current clinical dose of 4 mg/kg. Our results also highlight the continuing need for new therapeutic approaches for skeletal abnormalities in MPS VII, particularly those that target and modify the course of bone disease.

MATERIALS AND METHODS

Animals and study design

For this study, we used the naturally occurring canine model of MPS VII. MPS VII dogs have a missense mutation (R166H) in the GUSB gene³³ and exhibit a similar skeletal phenotype to human patients, including abnormalities in the vertebral bones and synovial joints.^{8,21,33} The original MPS VII dog was of mixed breed and thought to be of German shepherd descent,^{33,34} and has since been further outbred. Animals were raised and housed at the Referral Center for Animal Models of Human Genetic Disease at University of Pennsylvania School of Veterinary Medicine under NIH and USDA guidelines for the care and use of animals in research. A total of 23 animals were used and all studies were carried out with approval from the Institutional Animal Care and Use Committee of the University of Pennsylvania. Animals were housed in kennel runs in groups of 2 or 3, with a light cycle of 12 h per day, an ambient temperature of 21°C (29°C for whelping), with food and water provided ad libitum. MPS VII dogs were treated with intravenous vestronidase alfa (UX003; Ultragenyx Pharmaceutical Inc., Novato, CA) beginning at age 2 days. Two doses were evaluated: the standard clinical dose of 4 mg/kg (“MPS VII ERT SD,” n = 5, 3 males and 2 females) and a high dose of 20 mg/kg (“MPS VII ERT HD,” n = 3, 2 males and 1 female). Study groups also included untreated MPS VII animals (“MPS VII Untreated,” n = 6, 1 male and 5 females) and healthy controls (“Controls,” n = 6, 2 males and 4 females). Genotypes were established via variant-specific real-time PCR analysis at birth. Control and MPS VII dogs were heterozygous and homozygous for the GUSB mutation, respectively. Heterozygous animals are phenotypically normal. Vestronidase alfa was stored at 4°C and dosing formulations were prepared biweekly, immediately prior to injection. Bolus (“slow push”) administrations were given at age 2 and 9 days (the second timed to coincide with the commencement of secondary ossification¹⁰), the first 2-h infusion performed at age 23 days, and subsequent infusions every 14 days (consistent with current clinical protocols). For the 2-h infusion, vestronidase alfa was administered at a rate of 3 mL/kg/h over the first hour, and at a rate of 7 mL/kg/h over the second hour, consistent with current clinical protocols. Bolus administrations were performed at age 2 and 9 days as the small size of the animals made infusions impractical. For the 4 mg/kg dose, drug was diluted from a 2 mg/mL stock to the working concentration in sterile saline. For the 20 mg/kg dose undiluted stock enzyme was injected. Animals were weighed twice weekly and enzyme dosage adjusted accordingly. Based on adverse reactions (nausea, vomiting, and diarrhea) that occurred during pilot studies using the 4 mg/kg dose, a prophylactic drug regimen was developed, and administered immediately prior

to ERT for all treated animals. These drugs included diphenhydramine (4 mg/kg, an antihistamine), and ondansetron and maropitant citrate (0.2 and 2 mg/kg, respectively, both antiemetics). For ERT HD animals, this regime was not sufficient to prevent adverse reactions, and a prophylactic steroid, dexamethasone (up to 0.6 mg/kg) was also required as an immunosuppressant. No further adverse events because of ERT occurred with this prophylactic drug regimen in place. Given the known anti-inflammatory properties of dexamethasone, in order to determine whether administration of this steroid alone impacted synovial joint disease, an additional study group of MPS VII animals (“MPS VII Steroid Control,” n = 3, 2 males and 1 female) was subsequently included, which received all prophylactic drugs but not ERT according to the same schedule. *In vivo* assessments included plain radiographs of the lumbar spine and lower appendicular skeleton at age 3 and 6 months, monthly physical examinations, and complete blood chemistry analysis. Animals were euthanized at age 6 months via an overdose of sodium pentobarbital. Euthanasia was performed 24 h after the final enzyme infusion. This period was selected to ensure exogenous circulating enzyme would not confound tissue-level assessments of enzyme levels, given the reported short plasma half-life of vestronidase alfa in patients of approximately 2.5 h^{35,36}. Postmortem analyses included tissue enzyme distribution and GAG content for major organ systems, expression of inflammatory mediators in synovial fluid and serum, MRI of stifle joints, biomechanical testing of CCLs, microCT of vertebral bodies, and histological evaluation of both articular cartilage and vertebral bodies. For MPS VII steroid control animals, outcomes were limited to clinical evaluations, imaging, and bloodwork; full necropsies for these animals were not possible to pandemic-associated university shutdowns.

Clinical evaluations

All animals received a monthly full physical examination from a veterinarian (M.L.C.), including comprehensive evaluation of skeletal disease progression and mobility status. Monthly weight measurements were obtained. Blood samples were collected from each animal at age 6 months (immediately prior to euthanasia) from the cephalic vein. Collected blood was placed into serum-separating tubes and let sit for 30 min at room temperature until the blood had clotted. The tube was placed into a centrifuge and spun at 1,000 × g for 10 min and serum collected. Samples were submitted for complete blood cell counts and serum chemistry analysis at the Clinical Pathology Core at the Ryan Veterinary Hospital of the University of Pennsylvania School of Veterinary Medicine. Remaining aliquots were snap frozen in liquid nitrogen and stored at −80°C until required for the assessment of inflammatory mediators and BAP as described below.

Tissue enzyme distribution and GAG content

GUSB and HEX activities and GAG content were measured in the following tissues: articular cartilage (from stifle joints), synovial membrane (stifle joint), brain (hippocampus, brain stem and frontal lobe), spinal cord (cervical, lumbar and thoracic), aorta (ascending and descending), heart muscle, liver, spleen, and kidney (cortex and medulla). Tissue samples were collected postmortem, flash frozen and stored at −80°C. Prior to assays being conducted, samples were

thawed, weighed, suspended in a homogenization buffer containing 0.2% Triton X-100 and 0.9% saline, and homogenized using a Kinematica Polytron homogenizer for 30–45 s on ice. Homogenates were then centrifuged at 12,000 rcf for 20 min. The clear supernatant was then transferred to new tubes, and total protein quantified using the bicinchoninic acid assay (Sigma-Aldrich, CA). GUSB activity was measured using standard techniques with 4-methylumbelliferyl β -D-glucuronide (Sigma-Aldrich) as the substrate, while HEX activity was assayed using 4-methylumbelliferyl N-acetyl- β -D-glucosaminide (Sigma-Aldrich) as the substrate.³⁷ Results for both were expressed as nM/h/mg protein. Soluble sulfated GAG content in homogenized tissue sample supernatants was determined using the commercial Blyscan assay (Bicolor, Ireland). Results were normalized to total protein. Total sulfated GAG was also measured in serum collected prior to euthanasia at age 6 months, and expressed as $\mu\text{g/mL}$.

Inflammatory mediators in synovial fluid and serum

Inflammatory mediator analysis was performed on synovial fluid and serum samples collected on the day of euthanasia (at age 6 months) using a 37-plex immunoassay kit (Bio-Plex Pro Human Inflammation Panel 1, cat. no. 171AL001M, Bio-Rad, Hercules, CA). Pilot experiments were performed to confirm cross-reactivity with canine samples. Serum and synovial fluid sample aliquots were thawed and diluted 1:4 in sample diluent buffer, and assays run using a Bio-Plex 200 System (Bio-Rad) as per the manufacturer's instructions. Molecules that returned an out-of-range (undetectable) reading were excluded from analyses.

Imaging

Lateral plain radiographs of lumbar spines, and left and right hindlimbs, were obtained *in vivo* at age 3 and 6 months. Animals were sedated using intramuscular hydromorphone and atropine followed by intravenous propofol for short-term anesthesia. Radiographs were reviewed and interpreted by the attending veterinary radiologist. The presence or absence of each of the following parameters was noted and summarized by study group: underdeveloped vertebral epiphyses, vertebral shortening, shallow or irregular acetabula, genu valgum, tibial bowing, limb muscle atrophy, coxofemoral luxation, and femoral epiphyseal irregularities.

MRI of left canine stifle joints (with musculature and skin intact) was performed *ex vivo* at age 6 months. Before imaging, hindlimbs were thawed overnight at 4°C and brought to room temperature. Images were acquired with a 3T MR scanner (Magnetom Trio with TIM system; Siemens Healthcare, Malvern, PA) using a four-channel small flex coil, with the limb in the right lateral position and the stifle joint at an anatomical angle of 135°. The following sequences were acquired: proton density-weighted (TR/TE = 3,900/40 ms); T2-weighted with fat suppression (TR/TE = 8,050/77 ms); and T1-weighted volumetric interpolated breath-hold examination with water excitation (TR/TE = 10.4/4.9 ms). The slice thickness was 1.5 mm and field of view 140 mm for all three sequences. Images were acquired in both the sagittal and dorsal (coronal) planes. For semi-quantitative assessment

of joint pathology, in consultation with a board-certified veterinary radiologist (W.M.) a grading scheme was created for canine stifle joints by adapting elements from both the Knee Osteoarthritis Scoring System and MRI Osteoarthritis Knee Score schemes.^{39,40} The following parameters were assessed: effusion synovitis, Baker's cysts, meniscal degeneration, meniscal extrusion, patellar displacement, fat pad synovitis, bone marrow edema, cartilage defects, and subchondral cysts. Each parameter was assigned a grade from 0 (absent) to 3 (severe) by three independent, blinded assessors, with the average of individual scores calculated before statistical analyses. Overall grade was calculated as the sum of individual grades.

Biomechanical testing

Following MRI, left canine stifle joints from each group were opened and CCLs isolated by removing surrounding soft tissue while preserving osseous attachments to the distal femur and proximal tibia. Before mechanical testing, the cross-sectional area of the mid-substance of each CCL was measured with a custom laser-based measurement system.⁴¹ Femoral and tibial attachments were then potted in polymethyl methacrylate and mechanical testing was performed on a servo-hydraulic load frame (Instron 8874, Norwood, MA) equipped with a 10 kN load cell using an adaptation of previously published techniques.^{42–44} Custom aluminum fixtures were used to securely fix the osseous attachments at 45° of flexion (Figure 6A) and an X-Y linear stage was used to ensure the CCL was vertical under tensile loads less than 10 N. Before the onset of loading, the gauge length was measured with Vernier calipers. Samples were subjected to a pre-load of 10 N, followed by 15 cycles of preconditioning (1 mm peak-to-peak amplitude at 1 Hz). A ramp-to-failure was then performed under displacement control at a rate of 0.01 mm/s. Measures of time, force, and displacement were analyzed with custom software (MATLAB R2020a, MathWorks, Natick, MA). Testing was conducted at room temperature and samples were sprayed with saline to prevent dehydration. The following parameters were calculated for all samples: stiffness (N/mm), modulus (MPa), toughness (J/m^3), failure load (N), failure stress (N/mm^2), and failure strain (mm/mm).

MicroCT and bone turnover biomarker analysis

Whole T13 vertebral bodies were excised and fixed in 10% buffered formalin at 4°C for 1 week, then scanned using high-resolution microCT (VivaCT40; Scanco Medical AG, Brüttisellen, Switzerland). The entire region of trabecular bone within each vertebral primary ossification center bounded by the cranial and caudal primary spongiosa adjacent to the growth plates was segmented out, and sequential axial images were obtained with an isotropic voxel size of 19 μm , an integration time of 380 ms, peak tube voltage of 70 kV, current of 0.114 mA, and an acquisition of 1,000 projections per 180°. A three-dimensional Gaussian filter of 1.2 with a limited, finite filter support of 2 was used for noise suppression, and mineralized tissue was segmented from air or soft tissue using a threshold of 158.¹¹ To quantify bone content and architecture, standard three-dimensional morphometric analyses were performed using Scanco software to calculate bone volume fraction, BMD calibrated against hydroxyapatite (HA) standards (0–784 mg HA/cm³), trabecular

thickness, trabecular spacing, trabecular number, and connectivity density.¹¹ For bone turnover biomarker analysis, a 20- μ L total volume of undiluted serum was assayed for BAP activity using a MicroVue enzyme immunoassay kit (Quidel, San Diego, CA).

Histology

For examination of articular cartilage condition, following MRI, the distal femur was isolated from the stifle joint, fixed in 10% buffered formalin for 1 week, and completely decalcified in formic acid/ethylenediaminetetraacetic acid (Formical 2000; Statlab, Louisville, KY). A 3-mm-thick, mid-sagittal slice was then cut from the medial femoral condyle and processed into paraffin. Seven- μ m-thick sections were double stained with safranin-O and fast green and imaged under bright-field light microscopy (Eclipse 90i; Nikon, Tokyo, Japan). Semi-quantitative grading of cartilage condition was performed using an adaptation of the OARSI guidelines for dog osteoarthritis by three, independent, and blinded assessors.⁴⁵ The following parameters were determined: chondrocyte pathology, proteoglycan loss, cartilage structure, and overall grade (sum of individual parameters). Scoring incorporated assessments of both localized and global pathological changes across the width and depth of the condyle.⁴⁵ Scores from individual assessors were averaged prior to statistics.

For examination of vertebral bone, following microCT imaging, formalin-fixed T13 vertebrae were decalcified in formic acid/ethylenediaminetetraacetic acid. A 5-mm-thick mid-sagittal slab was then cut from each vertebra and processed for paraffin histology. Seven- μ m-thick sections were cut and double stained with either H&E to demonstrate cellularity or Alcian blue and picosirius red (ABPR) for GAGs and collagen, respectively.¹¹ Sections were imaged under bright-field light microscopy. The presence of cartilaginous lesions in secondary ossification centers was qualitatively assessed from ABPR-stained sections. Growth plate morphology was quantitatively assessed using mid-sagittal H&E-stained sections as described previously.¹¹ Total numbers of proliferating and hypertrophic chondrocytes were manually counted in a standardized 1-mm-wide region in the center of the growth plate and normalized to total area (NIS-Elements software; Nikon, Tokyo, Japan). The mean heights of the proliferating and hypertrophic zones were determined from the same standardized regions. Results from the cranial and caudal growth plates for each vertebra were averaged prior to statistical analyses.

Statistical analyses

All statistical analyses were performed using GraphPad Prism 8.4 (GraphPad Software, San Diego, CA). Significant differences between study groups for all quantitative outcome measures were established using Kruskal-Wallis multiple comparisons tests with pairwise differences established using post-hoc Dunn's tests. Significance was defined as $p < 0.05$. All results are presented as median and interquartile range.

DATA AVAILABILITY STATEMENT

The data supporting the studies presented in this manuscript can be found in the main text or the [supplemental information](#). Additional

information may be made available upon reasonable request to the corresponding authors as appropriate.

SUPPLEMENTAL INFORMATION

Supplemental information can be found online at <https://doi.org/10.1016/j.omtm.2022.11.006>.

ACKNOWLEDGMENTS

Funding for this work was received from Ultragenyx Pharmaceutical Inc and the National Institutes of Health (R01AR071975, P40OD010939, and P30AR069619). Vestronidase alfa was provided by Ultragenyx Pharmaceutical. Animal care provided by the staff and students of the Referral Center for Animal Models of Human Genetic Disease at the University of Pennsylvania, in particular Dr Jessica Bagel, Patricia O'Donnell, and Caitlyn Molony, is gratefully acknowledged. Technical support provided by the biomechanics, microCT, and histology cores of the Penn Center for Musculoskeletal Disorders, and by the Large Animal Imaging Facility at the University of Pennsylvania is gratefully acknowledged.

AUTHOR CONTRIBUTIONS

R.G. and Y.K.L. contributed to study design, performed experiments, interpreted findings, and drafted the manuscript. L.J.S. conceived the study, contributed to study design, interpreted findings, and drafted the manuscript. M.L.C. contributed to study design, performed physical examinations, interpreted findings, and drafted the manuscript. G.R.D. contributed to the design and implementation of histology and multiplex immunoassay experiments, and interpretation of findings. W.M. contributed to the design, implementation, and interpretation of imaging studies. S.S.S. contributed to design of biomechanical studies and performed experiments. C.R.S., S.Y.J., G.L., C.Z., Z.J., and K.A. performed the experiments. All authors provided critical feedback on the manuscript and approved the final version prior to submission.

DECLARATION OF INTERESTS

This study was funded in part by Ultragenyx Pharmaceutical, the company that produces vestronidase alfa (the drug that was evaluated). In addition, the drug used in the study was provided by the company at no cost to the investigators. Specific author conflicts: L.J.S., Research grant from Ultragenyx Pharmaceutical; Scientific Advisory Board, National MPS Society; Scientific Advisory Board, JOR Spine. G.R.D., co-founder and CEO, Mechano-Therapeutics LLC. W.M., book royalties, "Diagnostic MRI in Dogs and Cats," Taylor & Francis. R.G., consultant, Acorn Biolabs; Scientific Advisory Board, JOR Spine. C.R.S., G.L., C.Z., Z.J., Y.K.L., S.S.S., S.Y.J., and K.A., no relevant disclosures.

REFERENCES

1. Neufeld, E.F., and Muenzer, J. (2001). The mucopolysaccharidoses. In *The Metabolic and Molecular Bases of Inherited Disease*, C.R. Scriver, A.L. Beaudet, W.S. Sly, and D. Valle, eds. (McGraw-Hill), pp. 3421–3452.

2. Puckett, Y., Mallorga-Hernández, A., and Montaña, A.M. (2021). Epidemiology of mucopolysaccharidoses (MPS) in United States: challenges and opportunities. *Orphanet J. Rare Dis.* 16, 241.
3. Sly, W.S., Quinton, B.A., McAlister, W.H., and Rimoin, D.L. (1973). Beta glucuronidase deficiency: report of clinical, radiologic, and biochemical features of a new mucopolysaccharidosis. *J. Pediatr.* 82, 249–257.
4. Montaña, A.M., Lock-Hock, N., Steiner, R.D., Graham, B.H., Szlago, M., Greenstein, R., Pineda, M., Gonzalez-Meneses, A., Çoker, M., Bartholomew, D., et al. (2016). Clinical course of sly syndrome (mucopolysaccharidosis type VII). *J. Med. Genet.* 53, 403–418.
5. White, K.K. (2011). Orthopaedic aspects of mucopolysaccharidoses. *Rheumatology* 50 (Suppl 5), v26–v33.
6. Jiang, Z., Byers, S., Casal, M.L., and Smith, L.J. (2020). Failures of endochondral ossification in the mucopolysaccharidoses. *Curr. Osteoporos. Rep.* 18, 759–773.
7. Peck, S.H., Casal, M.L., Malhotra, N.R., Ficiocioglu, C., and Smith, L.J. (2016). Pathogenesis and treatment of spine disease in the mucopolysaccharidoses. *Mol. Genet. Metab.* 118, 232–243.
8. Smith, L.J., Baldo, G., Wu, S., Liu, Y., Whyte, M.P., Giugliani, R., Elliott, D.M., Haskins, M.E., and Ponder, K.P. (2012). Pathogenesis of lumbar spine disease in mucopolysaccharidosis VII. *Mol. Genet. Metab.* 107, 153–160.
9. Jiang, Z., Lau, Y.K., Wu, M., Casal, M.L., and Smith, L.J. (2021). Ultrastructural analysis of different skeletal cell types in mucopolysaccharidosis dogs at the onset of post-natal growth. *J. Anat.* 238, 416–425.
10. Peck, S.H., O'Donnell, P.J.M., Kang, J.L., Malhotra, N.R., Dodge, G.R., Pacifici, M., Shore, E.M., Haskins, M.E., and Smith, L.J. (2015). Delayed hypertrophic differentiation of epiphyseal chondrocytes contributes to failed secondary ossification in mucopolysaccharidosis VII dogs. *Mol. Genet. Metab.* 116, 195–203.
11. Peck, S.H., Lau, Y.K., Kang, J.L., Lin, M., Arginteanu, T., Matalon, D.R., Bendigo, J.R., O'Donnell, P., Haskins, M.E., Casal, M.L., and Smith, L.J. (2021). Progression of vertebral bone disease in mucopolysaccharidosis VII dogs from birth to skeletal maturity. *Mol. Genet. Metab.* 133, 378–385.
12. Simonaro, C.M., D'Angelo, M., Haskins, M.E., and Schuchman, E.H. (2005). Joint and bone disease in mucopolysaccharidoses VI and VII: identification of new therapeutic targets and biomarkers using animal models. *Pediatr. Res.* 57, 701–707.
13. Simonaro, C.M., D'Angelo, M., He, X., Eliyahu, E., Shtraizent, N., Haskins, M.E., and Schuchman, E.H. (2008). Mechanism of glycosaminoglycan-mediated bone and joint disease: implications for the mucopolysaccharidoses and other connective tissue diseases. *Am. J. Pathol.* 172, 112–122.
14. Chen, H.H., Sawamoto, K., Mason, R.W., Kobayashi, H., Yamaguchi, S., Suzuki, Y., Orii, K., Orii, T., and Tomatsu, S. (2019). Enzyme replacement therapy for mucopolysaccharidoses; past, present, and future. *J. Hum. Genet.* 64, 1153–1171.
15. Fox, J.E., Volpe, L., Bullaro, J., Kakkis, E.D., and Sly, W.S. (2015). First human treatment with investigational rhGUS enzyme replacement therapy in an advanced stage MPS VII patient. *Mol. Genet. Metab.* 114, 203–208.
16. Wang, R.Y., da Silva Franco, J.F., López-Valdez, J., Martins, E., Sutton, V.R., Whitley, C.B., Zhang, L., Cimmis, T., Marsden, D., Jurecka, A., and Harmatz, P. (2020). The long-term safety and efficacy of vestronidase alfa, rhGUS enzyme replacement therapy, in subjects with mucopolysaccharidosis VII. *Mol. Genet. Metab.* 129, 219–227.
17. Lau, H.A., Viskochil, D., Tanpaiboon, P., Lopez, A.G.M., Martins, E., Taylor, J., Malkus, B., Zhang, L., Jurecka, A., and Marsden, D. (2022). Long-term efficacy and safety of vestronidase alfa enzyme replacement therapy in pediatric subjects < 5 years with mucopolysaccharidosis VII. *Mol. Genet. Metab.* 136, 28–37.
18. Sands, M.S., Vogler, C., Kyle, J.W., Grubb, J.H., Levy, B., Galvin, N., Sly, W.S., and Birkenmeier, E.H. (1994). Enzyme replacement therapy for murine mucopolysaccharidosis type VII. *J. Clin. Invest.* 93, 2324–2331.
19. Haskins, M.E. (2007). Animal models for mucopolysaccharidosis disorders and their clinical relevance. *Acta Paediatr.* 96, 56–62.
20. Smith, L.J., Martin, J.T., Szczesny, S.E., Ponder, K.P., Haskins, M.E., and Elliott, D.M. (2010). Altered lumbar spine structure, biochemistry, and biomechanical properties in a canine model of mucopolysaccharidosis type VII. *J. Orthop. Res.* 28, 616–622.
21. Xing, E.M., Knox, V.W., O'Donnell, P.A., Sikura, T., Liu, Y., Wu, S., Casal, M.L., Haskins, M.E., and Ponder, K.P. (2013). The effect of neonatal gene therapy on skeletal manifestations in mucopolysaccharidosis VII dogs after a decade. *Mol. Genet. Metab.* 109, 183–193.
22. Byers, S., Nuttall, J.D., Crawley, A.C., Hopwood, J.J., Smith, K., and Fazzalari, N.L. (1997). Effect of enzyme replacement therapy on bone formation in a feline model of mucopolysaccharidosis type VI. *Bone* 21, 425–431.
23. Chiaro, J.A., O'Donnell, P., Shore, E.M., Malhotra, N.R., Ponder, K.P., Haskins, M.E., and Smith, L.J. (2014). Effects of neonatal enzyme replacement therapy and simvastatin treatment on cervical spine disease in mucopolysaccharidosis I dogs. *J. Bone Miner. Res.* 29, 2610–2617.
24. Harmatz, P., Whitley, C.B., Wang, R.Y., Bauer, M., Song, W., Haller, C., and Kakkis, E. (2018). A novel Blind Start study design to investigate vestronidase alfa for mucopolysaccharidosis VII, an ultra-rare genetic disease. *Mol. Genet. Metab.* 123, 488–494.
25. Cadaoas, J., Boyle, G., Jungles, S., Cullen, S., Vellard, M., Grubb, J.H., Jurecka, A., Sly, W., and Kakkis, E. (2020). Vestronidase alfa: recombinant human beta-glucuronidase as an enzyme replacement therapy for MPS VII. *Mol. Genet. Metab.* 130, 65–76.
26. Lund, T.C., Doherty, T.M., Eisengart, J.B., Freese, R.L., Rudser, K.D., Fung, E.B., Miller, B.S., White, K.K., Orchard, P.J., Whitley, C.B., and Polgreen, L.E. (2021). Biomarkers for prediction of skeletal disease progression in mucopolysaccharidosis type I. *JIMD Rep.* 58, 89–99.
27. Akioka, S. (2019). Interleukin-6 in juvenile idiopathic arthritis. *Mod. Rheumatol.* 29, 275–286.
28. Fonseca, J.E., Santos, M.J., Canhão, H., and Choy, E. (2009). Interleukin-6 as a key player in systemic inflammation and joint destruction. *Autoimmun. Rev.* 8, 538–542.
29. Narazaki, M., Tanaka, T., and Kishimoto, T. (2017). The role and therapeutic targeting of IL-6 in rheumatoid arthritis. *Expert Rev. Clin. Immunol.* 13, 535–551.
30. Wiegertjes, R., van de Loo, F.A.J., and Blaney Davidson, E.N. (2020). A roadmap to target interleukin-6 in osteoarthritis. *Rheumatology* 59, 2681–2694.
31. Ponder, K.P., Melniczek, J.R., Xu, L., Weil, M.A., O'Malley, T.M., O'Donnell, P.A., Knox, V.W., Aguirre, G.D., Mazrier, H., Ellinwood, N.M., et al. (2002). Therapeutic neonatal hepatic gene therapy in mucopolysaccharidosis VII dogs. *Proc. Natl. Acad. Sci. USA* 99, 13102–13107.
32. Smith, L.J., Martin, J.T., O'Donnell, P., Wang, P., Elliott, D.M., Haskins, M.E., and Ponder, K.P. (2012). Effect of neonatal gene therapy on lumbar spine disease in mucopolysaccharidosis VII dogs. *Mol. Genet. Metab.* 107, 145–152.
33. Haskins, M.E., Desnick, R.J., DiFerrante, N., Jezyk, P.F., and Patterson, D.F. (1984). Beta-glucuronidase deficiency in a dog: a model of human mucopolysaccharidosis VII. *Pediatr. Res.* 18, 980–984.
34. Haskins, M.E., Aguirre, G.D., Jezyk, P.F., Schuchman, E.H., Desnick, R.J., and Patterson, D.F. (1991). Mucopolysaccharidosis type VII (Sly syndrome). Beta-glucuronidase-deficient mucopolysaccharidosis in the dog. *Am. J. Pathol.* 138, 1553–1555.
35. Ultragenyx Pharmaceutical Inc (2017). MEPSEVII™ (vestronidase alfa-vjkb) pre-clinical information. https://www.accessdata.fda.gov/drugsatfda_docs/label/2017/761047s000lbl.pdf.
36. Qi, Y., McKeever, K., Taylor, J., Haller, C., Song, W., Jones, S.A., and Shi, J. (2019). Pharmacokinetic and pharmacodynamic modeling to optimize the dose of vestronidase alfa, an enzyme replacement therapy for treatment of patients with mucopolysaccharidosis type VII: results from three trials. *Clin. Pharmacokinet.* 58, 673–683.
37. Hommes, F.A. (1991). In *Techniques in Diagnostic Human Biochemical Genetics: A Laboratory Manual*, F.A. Hommes, ed. (Wiley-Liss), pp. 567–618.
38. Galindo-Zamora, V., Dziallas, P., Ludwig, D.C., Nolte, I., and Weststaedt, P. (2013). Diagnostic accuracy of a short-duration 3 Tesla magnetic resonance protocol for diagnosing stifle joint lesions in dogs with non-traumatic cranial cruciate ligament rupture. *BMC Vet. Res.* 9, 40.
39. Kornaat, P.R., Ceulemans, R.Y.T., Kroon, H.M., Riyazi, N., Kloppenburg, M., Carter, W.O., Woodworth, T.G., and Bloem, J.L. (2005). MRI assessment of knee osteoarthritis: knee Osteoarthritis Scoring System (KOSS)–inter-observer and intra-observer reproducibility of a compartment-based scoring system. *Skeletal Radiol.* 34, 95–102.
40. Hunter, D.J., Guermazi, A., Lo, G.H., Grainger, A.J., Conaghan, P.G., Boudreau, R.M., and Roemer, F.W. (2011). Evolution of semi-quantitative whole joint assessment of

- knee OA: MOAKS (MRI Osteoarthritis Knee Score). *Osteoarthritis Cartilage* 19, 990–1002.
41. Favata, M. (2006). Scarless Healing in the Fetus : Implications and Strategies for Postnatal Tendon Repair. Ph.D. Dissertation (University of Pennsylvania).
 42. Biskup, J.J., Balogh, D.G., Haynes, K.H., Freeman, A.L., and Conzemius, M.G. (2015). Mechanical strength of four allograft fixation techniques for ruptured cranial cruciate ligament repair in dogs. *Am. J. Vet. Res.* 76, 411–419.
 43. Dorlot, J.M., Ait Ba Sidi, M., Tremblay, G.M., and Drouin, G. (1980). Load elongation behavior of the canine anterior cruciate ligament. *J. Biomech. Eng.* 102, 190.
 44. Figgie, H.E., 3rd, Bahniuk, E.H., Heiple, K.G., and Davy, D.T. (1986). The effects of tibial-femoral angle on the failure mechanics of the canine anterior cruciate ligament. *J. Biomech.* 19, 89–91.
 45. Cook, J.L., Kuroki, K., Visco, D., Pelletier, J.P., Schulz, L., and Laféber, F.P.J.G. (2010). The OARSI histopathology initiative - recommendations for histological assessments of osteoarthritis in the dog. *Osteoarthritis Cartilage* 18, S66–S79.